Received: 15 April 2020 | Revised: 31 July 2020 | Accepted: 5 August 2020

DOI: 10.1002/hbm.25178

RESEARCH ARTICLE

WILEY

Resting theta activity is associated with specific coding levels in event-related theta activity during conflict monitoring

Charlotte Pscherer | Annet Bluschke | Astrid Prochnow | Elena Eggert | Moritz Mückschel | Christian Beste

Cognitive Neurophysiology, Department of Child and Adolescent Psychiatry, Faculty of Medicineof the TU Dresden, Dresden, Germany

Correspondence
Christian Beste, Cognitive Neurophysiology, Department of Child and Adolescent Psychiatry, Faculty of Medicine of the TU Dresden, Germany, Schubertstrasse 42, D-01309 Dresden, Germany.
Email: christian.beste@uniklinikum-dresden.de

Funding information
Collaborative Research Center/Transregio, Grant/Award Number: TRR 265; Deutsche Forschungsgemeinschaft, Grant/Award Number: SFB 940

Abstract

Brain electrical activity in the theta frequency band is essential for cognitive control (e.g., during conflict monitoring), but is also evident in the resting state. The link between resting state theta activity and its relevance for theta-related neural mechanisms during cognitive control is still undetermined. Yet, theoretical considerations suggest that there may be a connection. To examine the link between resting state theta activity and conflict-related theta activity, we combined temporal EEG signal decomposition methods with time-frequency decomposition and beamforming methods in N = 86 healthy participants. Results indicate that resting state theta activity is closely associated with the strength of conflict-related neural activity at the level of ERPs and total theta power (consisting of phase-locked and nonphase-locked aspects of theta activity). The data reveal that resting state theta activity is related to a specific aspect of conflict-related theta activity, mainly in superior frontal regions and in the supplemental motor area (SMA, BA6) in particular. The signal decomposition showed that only stimulus-related, but not motor-response-related coding levels in the EEG signal and the event-related total theta activity were associated with resting theta activity. This specificity of effects may explain why the association between resting state theta activity and overt conflict monitoring performance may not be as strong as often assumed. The results suggest that resting state theta activity is particularly important to consider for input integration processes during cognitive control.

KEYWORDS

conflict monitoring, EEG, resting state, source localization, theta

1 | INTRODUCTION

Brain electrical activity in the theta frequency band has been suggested to play a central role in cognitive control processes (Cavanagh & Frank, 2014; Cavanagh, Zambrano-Vazquez, & Allen, 2012; Cohen, 2014; De Blasio & Barry, 2013; Harper, Malone, & Bernat, 2014). The possible reason for this is that a large-power/low-frequency activity scheme is well-suited to orchestrate cognitive processes across distant brain areas (Buzsáki & Draguhn, 2004; Cavanagh & Frank, 2014). This orchestration is essential for efficient

cognitive control (Miller & Cohen, 2001). However, it is likely that theta band activity serves different computational roles, even within the cognitive control domain (Cohen, 2014).

One central instance of cognitive control is conflict monitoring (Botvinick, Braver, Barch, Carter, & Cohen, 2001; Botvinick & Cohen, 2014). It refers to situations where multiple response options are presented, but only one of them is the appropriate response. Such processes are typically examined using Flanker, Simon or Stroop tasks (Larson, Clayson, & Clawson, 2014). For conflict monitoring processes, it has been shown that especially the nonphase-locked portion of medial frontal theta activity is important to consider (Cohen, 2014; Nigbur, Cohen, Ridderinkhof, & Stürmer, 2012; Pastötter, Dreisbach, & Bäuml, 2013); that is, activity in the theta band that reflects burst-like dynamics during ongoing endogenous theta oscillations (Cohen, 2014). Because such endogenous activity is also characteristic for resting EEG activity across different frequency bands (Hiltunen et al., 2014; Knyazev, 2013; Laufs, 2008), there may be a link between resting theta band activity and theta-based activity evident during conflict monitoring. Such a link between resting state and task-related theta activity has already been shown for motor response inhibition (Pscherer, Mückschel, Summerer, Bluschke, & Beste, 2019). A more general link between resting activity and cognitive control-related activity is suggested by studies that revealed similarities between resting neural dynamics and task-related activity from a perspective of the involved neural networks (Becker, Van de Ville, & Kleinschmidt, 2018; Tavor et al., 2016). Some evidence suggests that there are links between resting state theta activity and event-related potential (ERP) indices of conflict monitoring (Nakao, Bai, Nashiwa, & Northoff, 2013). Yet, the links between resting state theta activity and EEG activity, as well as theta activity during cognitive control are still largely undetermined.

In this regard, it is very important to consider that ERP-components are composed of various amounts of signals from different sources (Huster, Plis, & Calhoun, 2015; Nunez et al., 1997; Stock, Gohil, Huster, & Beste, 2017) that are of particular relevance during response selection (Takacs et al., 2020; Takacs, Mückschel, Roessner, & Beste, 2020). Moreover, especially conflict monitoring requires the processing of different kinds of information or information coding levels. Already Folstein and Van Petten (2008) have suggested that motor-response-related processes are mixed with perceptual processes during conflict monitoring, especially at the time point of the N2 ERP, which is generated in the medial frontal cortex. This has, more recently, been corroborated by several studies using temporal EEG signal decomposition methods (Dippel, Mückschel, Ziemssen, & Beste, 2017; Mückschel, Chmielewski, Ziemssen, & Beste, 2017; Mückschel, Dippel, & Beste, 2017); that is, residue iteration decomposition (RIDE) (Ouyang, Sommer, & Zhou, 2015). Though RIDE has been developed to account for intra-individual variability in EEG data, it can also be used to dissociate stimulus-related processes from response- and decision-related processes during conflict monitoring (Mückschel, Chmielewski, et al., 2017). RIDE decomposes the EEG into three different clusters: an S-cluster reflecting stimulus-driven processes, an R-cluster reflecting motor response-related processes and an intermediate C-cluster reflecting stimulus–response transition and decision processes (Ouyang et al., 2015; Verleger, Grauhan, & Śmigasiewicz, 2016; Verleger, Metzner, Ouyang, Śmigasiewicz, & Zhou, 2014). Using RIDE, it has been shown that conflict monitoring processes in the N2 time window, as examined using a flanker task, are composed of activity in the S-cluster and the R-cluster and less so in the C-cluster (Mückschel, Chmielewski, et al., 2017). What has not been examined so far is the question of whether resting theta activity shows information-content specific associations with processes during conflict monitoring or interference control. This, however, is central to understand the relevance for resting state (theta) oscillatory activity and oscillatory activity during cognitive control. Some data suggest that particularly the processes reflected by the S-cluster in the N2 time window are quite specifically reflected by oscillations in the upper theta frequency band (Mückschel, Dippel, & Beste, 2017). For processes relating to the motor processes, the role of oscillatory activity is less clear-cut since oscillations in the entire theta band, as well as oscillations in lower frequency bands, seem to play a role (Mückschel, Dippel, & Beste, 2017). Based on these findings, the current study tests the hypothesis that resting state theta activity is closely associated with event-related theta activity during conflict monitoring.

To measure conflict monitoring, we used a flanker paradigm. We expect participants with relatively high resting theta activity to show stronger N2 amplitudes and higher event-related theta power during conflicting flanker trials than participants with lower resting theta activity. We hypothesize that these associations are particularly strong for stimulus-related processes (S-Cluster) during conflict monitoring in the N2 time window. This is all the more likely considering that EEG theta oscillations during conflict tasks have been suggested to reflect *input integration* processes that lead to the detection of conflict, rather than conflict monitoring per se (Cohen, 2014). Other subprocesses, also evident in that time window, are hence expected to show little or no association with resting state theta activity. Considering the functional neuroanatomical level, we further hypothesize that superior frontal and supplemental/premotor areas are associated with these modulatory effects in S-cluster related theta band activity. The reason is that superior frontal and supplemental/premotor areas have frequently been shown to process conflict-related information (Herz et al., 2014; Mars et al., 2009; Mückschel, Stock, Dippel, Chmielewski, & Beste, 2016; Nachev, Kennard, & Husain, 2008; Rushworth, Walton, Kennerley, & Bannerman, 2004; Stock, Wascher, & Beste, 2013). Interestingly, these areas have previously been associated with modulations of the S-cluster during conflict monitoring (Mückschel, Chmielewski, et al., 2017). Moreover, also EEG beamforming data suggest that oscillations in the upper theta frequency band reflecting stimulus-related processes during cognitive control are associated with superior frontal areas (Mückschel, Dippel, & Beste, 2017).

The expected data pattern would suggest that resting state activity in the theta frequency band has a very specific effect on neuronal processes of conflict monitoring. Resting state theta activity would only be relevant for some subprocesses during conflict monitoring and would not have a cross-coding level effect on conflict monitoring

mechanisms. This would further specify the relevance of nonphase locked theta activity and neural mechanisms during conflict monitoring.

2 | MATERIALS AND METHODS

2.1 | Power calculation and participants

In our study, we hypothesized that there are interactive effects between the resting theta level as the between-subjects factor ("group": $rtheta_{high}$ vs. $rtheta_{low}$) and the conflict level of the flanker trials as the within-subject factor ("congruency": congruent vs. incongruent). To compare participants with a relatively high resting theta level ($rtheta_{high}$) to subjects with a relatively low resting theta level ($rtheta_{low}$), we planned to perform a median split. For this purpose, we aimed to analyze our data with mixed-effects ANOVAs. We used G*Power (Faul, Erdfelder, Lang, & Buchner, 2007) to estimate the required sample size to obtain small effect sizes (partial eta squared η_p^2) of .05 with a power of 95%. A moderate inter-correlation between repeated measures was assumed. We conservatively considered small effect sizes since we were not aware of comparable data to rely on for effect size estimation. This a-priori effect size estimation revealed a required sample size of at least $N = 64$ subjects. To provide a full picture of the data, we additionally examined whether there are linear inter-relations between resting state theta band activity and conflict monitoring, as well as conflict-related theta activity by calculating linear correlations. For such analyses, the power calculation (sensitivity analysis) revealed that correlations of $r \sim .3$ can reliably be estimated with a power of 90% and a sample size of $N = 90$ at an alpha level of $p = .05$.

Therefore, the recruited sample for the current study included $N = 93$ healthy, right-handed adults between 18 and 40 years of age. About 70% of this sample also participated in a previous study of our research group investigating resting theta activity with a different task (Pscherer et al., 2019). In the present sample, we defined two groups based on the median value of the participants' resting theta activity. As explained above, this median split resulted in a $rtheta_{high}$ and a $rtheta_{low}$ group. Details on how resting theta activity was assessed are described in Section 2.2. Due to technical problems and data with the exact median value, we excluded the data of seven participants. The final sample consisted of $N = 86$ participants (45 male, age: 26.02 ± 4.63, IQ: 111.70 ± 12.75). The two groups ($rtheta_{high}$ vs. $rtheta_{low}$) did not differ significantly regarding age ($t[84] = -0.23$, $p = .817$) and IQ ($t[84] = 0.62$, $p = .535$). All participants provided written informed consent and received a financial reimbursement for their study participation. The ethics committee of the TU Dresden approved this study.

2.2 | Assessment of resting theta activity

To assess the participants' resting theta activity, we used the same setup as in a previous study (please refer to Pscherer et al., 2019 for details). The subjects' brain electrical activity was continuously recorded at electrode Cz. Electrodes above and below the right eye were applied to record and correct for strong eye movement or blinking artifacts. A reference electrode was placed on the right earlobe and an electrode on the forehead served as ground electrode. An online Butterworth filter was applied to determine theta power in the frequency range of 4–7 Hz. To measure resting theta activity, participants were asked to relax for 2 min with their eyes open. The participants' individual average resting theta band activity in this two-min time-interval was used to calculate a median split and divide the sample into a group with a relatively low resting theta activity ($rtheta_{low}$) and a group with a relatively high resting theta activity ($rtheta_{high}$). The subjects' individual average resting theta band activity was also used in the additional correlation analyses.

2.3 | Task

After measuring the resting theta activity, we instructed the participants to perform a standard flanker task for the assessment of conflict monitoring. For this purpose, a target stimulus (white arrowhead) was presented in the center of a black screen, either pointing left or right. It was vertically flanked by two adjacent white distractor arrowheads. These flanker stimuli either pointed in the same direction (congruent condition) or in the opposite direction (incongruent condition) as the target stimulus. Participants were requested to press the left button of a response pad with their left index finger when the target stimulus pointed to the left and the right button with their right index finger when the target stimulus pointed to the right. The flanker stimuli preceded the target stimulus with a stimulus-onset asynchrony of 200 ms. The target arrowhead was presented for 300 ms after which target and flanker stimuli were switched off simultaneously. To exert time pressure, participants were asked to respond within a time-interval of 600 ms after stimulus onset. If this time limit was exceeded, an auditory feedback tone (1,000 Hz, 60 dB SPL) was presented 1,200 ms after stimulus onset. The flanker task consisted of four blocks with 120 trials each (67% congruent, 33% incongruent).

2.4 | EEG recording and analysis

While participants were performing the flanker task, an EEG was recorded from 60 equidistant electrodes using BrainVision Recorder 2.1 (Brain Products Inc.). Electrode impedances were kept below 5 kΩ. The ground electrode was placed at $\theta = 58$, $\phi = 78$, the reference electrode at $\theta = 90$, $\phi = 90$. The BrainVision Analyzer 2.1 software package (Brain Products Inc.) was used for offline data processing. The experimenter who preprocessed the data was blind to the resting theta level of the participants. First, we down-sampled the data to 256 Hz and applied an IIR-band-pass filter from 0.5 to 20 Hz with a slope of 48 db/oct, as well as a notch filter of 50 Hz. By means of a manual raw data inspection, offsets in the EEG like technical and muscular artifacts were removed. We applied an independent

component analysis (ICA, infomax algorithm) to identify and manually remove eye movements, blinks, pulse and muscular artifacts. Afterward, the data were segmented and locked to the onset of congruent and incongruent target stimuli, separately. Each segment had a length of 4,000 ms (2,000 ms before until 2,000 ms after onset of the target stimulus) to provide a time interval which is long enough for a reliable analysis of theta frequency band activity (Yordanova, Falkenstein, Hohnsbein, & Kolev, 2004). By means of an automated artifact rejection, trials in which the maximal amplitude exceeded 150 μV or −150 μV were excluded from the data. Furthermore, trials with a maximal value difference of 200 μV in an interval of 200 ms or with an activity below 0.5 μV in a 100 ms interval were removed. To obtain a reference-free representation of the data and to provide an improved localization of the electrical activity on the scalp, we applied a current source density (CSD) transformation (Nunez & Pilgreen, 1991) with 4 splines and 10 polynomials. Next, we performed a baseline correction in the time window from −400 to −200 ms before the onset of the target stimulus. For analysis of the ERP components, the segments of each participant were averaged for congruent and incongruent trials, separately. To define the ERP component N2, we visually inspected the scalp topographies of the grand averages. The N2 was quantified at electrode Cz in the time interval between 240 and 260 ms after the onset of the target stimulus. This time window was centered around the component peak. The mean amplitude of the N2 component during the short time window was determined on a single-subject level for both conditions.

2.5 | Residue iteration decomposition

A classical ERP signal is obtained by averaging various single trials. Since the signal latencies vary from trial to trial, the average ERP signal is prone to be smeared (Ouyang et al., 2015). RIDE is a method to decompose the standard ERP signal into component clusters based on their latency variability and thereby prevents the signal from being smeared (Ouyang et al., 2015). These component clusters are furthermore a possibility to split the ERP signal into separate clusters that are associated with different stages of cognitive processing (Ouyang et al., 2015). Using the RIDE toolbox (available on http://cns.hkbu.edu.hk/RIDE.htm), one can decompose the single-trial ERP data into components with static latency (S- and R-clusters) and variable latency (C-cluster). The S-cluster is locked to the onset of the target stimulus presentation and therefore reflects stimulus-driven processes (Ouyang et al., 2015). Cognitive processes related to motor response are represented by the R-cluster, which is locked to the response onset (Ouyang et al., 2015). The central C-cluster is associated with stimulus–response transition and decision-making. Since this intermediate cluster is neither locked to the stimulus nor to the response, it must be estimated initially and is then improved by an iteration procedure (Ouyang et al., 2015). To extract the waveform of each component, RIDE uses a time window function. For a start, time windows have to be chosen in a range that covers the assumed occurrence of each component. In this study, we chose time intervals from 200 ms before to 500 ms after target stimulus onset for the S-cluster, from 100 to 900 ms after target stimulus onset for the C-cluster and ±300 ms around the response for the R-cluster. The chosen time intervals are comparable to previously used time windows in a RIDE study examining Flanker data (Mückschel, Chmielewski, et al., 2017). RIDE uses these time markers as initial estimates for the decomposition of the ERP components. The component latencies are then adjusted iteratively. For every step, RIDE estimates each component separately by subtracting the other two components from each single trial (Ouyang et al., 2015). Next, it uses L1-norm minimization to obtain a median waveform for each component cluster for all trials (Ouyang et al., 2015). These steps are repeated until the component latencies converge. For further details on the methodological principals of RIDE, please refer to (Ouyang et al., 2015; Ouyang, Herzmann, Zhou, & Sommer, 2011). After applying the RIDE method, we generated the grand averages of all participants for all three component clusters. As with the original ERP data (see Section 2.4), electrode sites for the peak quantification were determined by visual inspection of the grand average scalp topographies. In the S-cluster, we observed activity in the time window of the N2 component. The mean amplitude was determined at electrodes Cz (250–265 ms) and FCz (260–270 ms). The C-cluster revealed activity in the N2 and P3 time intervals with mean amplitudes quantified at electrodes Cz, FCz (N2: 220–240 ms), Pz and P2 (P3 for congruent trials: 280–340 ms, P3 for incongruent trials: 370–410 ms). The R-cluster also showed activity in the time window of N2. We determined its mean activity at electrode Cz (N2 for congruent trials: 270–280 ms, N2 for incongruent trials: 370–390 ms). Due to a latency shift, the peaks of the N2 component in the R-Cluster and of the P3 component in the C-cluster differed for the congruent and incongruent conditions. For this reason, separate analysis windows were quantified for each condition in these cases. The mean amplitudes for each component and both conditions (congruent vs. incongruent) were used for statistical analysis.

2.6 | Time-frequency analysis

We computed time-frequency (TF) analyses to examine theta frequency band activity during the flanker task in detail. To analyze total theta power consisting of phase-lo×cked and nonphase-locked aspects of theta power, TF analysis was applied on single-trial data of each participant for congruent and incongruent condition. We also applied a TF analysis on the single-trial RIDE data of each participant for the S-cluster in both conditions. As the N2 component in R- and C-cluster revealed no significant interaction effects *group* × *condition* (see Section 3.2.3), we did not analyze TF decomposition for these clusters and restricted the analysis to the S-cluster. To compute TF analyses, we applied Morlet wavelets (w):

$$w(t,f) = A\exp\left(-t^2/2\sigma_t^2\right)\exp(2i\pi ft)$$

with the parameters t = time, f = frequency, $A = (\sigma_t\sqrt{\pi})^{-1/2}$, σ_t = wavelet duration, and $i = \sqrt{-1}$. A Morlet parameter of $f_0/\sigma_f = 5.5$ was used,

with f_0 representing the central frequency and σ_f defining the Gaussian shape in the frequency domain. TF decomposition was performed in a frequency range from 0.5 to 20 Hz in 40 steps of 0.5 Hz. Wavelet duration can be calculated as $2\sigma_t$ and spectral band width can be calculated as $2\sigma_f$ for different f_0. The equation $\sigma_t = 1/(2\pi\sigma_f)$ relates the parameters σ_t and σ_f. After computing TF analyses, we identified maximal total theta power based on visual inspection of the grand average scalp topographies. Maximal theta power was determined at electrode Cz in the frequency band of 6.5 Hz in the time window between 100 and 400 ms after onset of the target stimulus. In this time window, maximal theta power for the statistical analysis was detected automatically.

2.7 | Beamforming analysis

The beamforming analysis was computed to identify the neuroanatomical regions associated with group differences in task-related theta activity. For the beamforming analysis, no CSD transformation was applied beforehand, because the beamformer itself works as a spatial filter. Rather, we used average referenced data and applied a dynamic imaging of coherent sources (DICS) beamformer (Gross et al., 2001). To compute the power and the cross spectral density matrix, a multitaper frequency transformation was applied. Then, theta band frequency at 6.5 Hz was selected and a smoothing window of ±1.67 Hz was applied, which corresponds to the frequency range identified for the electrode-level TF-analysis. Using the forward model and the MNI brain template implanted in Fieldtrip, the beamformer was calculated (see: Oostenveld, Stegeman, Praamstra, and van Oosterom (2003). A detailed description of the forward model construction is provided by Oostenveld, Fries, Maris, and Schoffelen (2010). After realigning the EEG electrodes to the forward model, the forward model's brain volume was partitioned into a grid with 6 mm resolution for the leadfield matrix computation. The leadfield matrix was then calculated for each grid point. The beamformed time-frequency window was chosen based on the findings of theta band activity, which revealed a maximum between 100 and 400 ms after the target stimulus onset (see above). The time-frequency window was set at 100–700 ms at a core frequency of 6.5 Hz ±1.67 Hz. This ensures that the DICS beamformer was based on at least three full cycles. For each group (i.e., $\text{rtheta}_{\text{high}}$ group and $\text{rtheta}_{\text{low}}$ group), a spatial filter with the regularization parameter set to 5% was applied in the incongruent condition to estimate the power of the sources.

2.8 | Statistical analysis

We used SPSS Statistics 25 to analyze behavioral and neurophysiological data. Mixed-effects ANOVA analyses were computed with the within-subject factor "congruency" (congruent vs. incongruent trials) and the between-subjects factor "group" ($\text{rtheta}_{\text{low}}$ vs. $\text{rtheta}_{\text{high}}$). For analysis of the ERPs and the RIDE data, we additionally used the within-subject factor *"electrode"* whenever necessary. All posthoc tests were Bonferroni-corrected and computed with one-tailed t-tests. For descriptive statistics, mean and standard error of the mean are given. Moreover, we analyzed linear correlations between resting theta activity and several neurophysiological outcome variables with Pearson's correlation coefficient *r*. We used bootstrapping to provide 95% confidence intervals (CI) for the correlation coefficients. Furthermore, we conducted Bayesian Pearson correlation tests with JASP (Love et al., 2019) in cases with significant results in one condition (congruent/incongruent), but not in the other condition, to examine a possible dissociation in the pattern of correlations between conditions.

3 | RESULTS

Our sample of $N = 86$ participants was split at the median value of resting theta activity ($\tilde{x} = 3.39\ \mu V/m^2$) into a group with relatively low resting theta activity ($\text{rtheta}_{\text{low}}$, $n = 43$, $2.95\ \mu V/m^2 \pm 0.04$) and a group with relatively high resting theta activity ($\text{rtheta}_{\text{high}}$, $n = 43$, $3.81\ \mu V/m^2 \pm 0.05$). The results of the analysis of behavioral and neurophysiological differences between these two groups are presented below. Additionally, we calculated correlation analyses between resting state theta activity and task-related neurophysiological activity during conflict monitoring (see Section 3.2.5).

3.1 | Behavioral data

The mixed-effects ANOVA revealed significant main effects of *congruency* for both the percentage of correct hits ($F_{(1,84)} = 184.66$, $p < .001$, $\eta p^2 = .69$) and reaction time (RT, $F_{(1,84)} = 968.47$, $p < .001$, $\eta p^2 = .92$). During congruent trials, participants responded more accurately (96% ± 3) and faster (271 ms ± 3) than during incongruent trials (hit rate: 81% ± 1, RT: 358 ms ± 3). There were no significant interaction effects or main effects with the factor *group* (all $F < 0.64$, all $p > .425$).

3.2 | Neurophysiological data

3.2.1 | Standard ERPs

For the standard ERPs, we examined the N2 ERP-component at electrode Cz. The mixed-effects ANOVA revealed a significant interaction of *congruency* × *group* for the N2 ($F_{(1,84)} = 4.74$, $p = .032$, $\eta p^2 = .05$), which is illustrated in Figure 1a.

Posthoc tests showed that there was a main effect of *group* during incongruent trials ($t(84) = 1.95$, $p = .05$, $d = -0.42$). In the incongruent condition, the $\text{rtheta}_{\text{high}}$ group showed a larger N2 amplitude ($-17.76\ \mu V/m^2 \pm 2.53$) than the $\text{rtheta}_{\text{low}}$ group ($-11.49\ \mu V/m^2 \pm 1.99$). During congruent trials, N2 amplitudes of the $\text{rtheta}_{\text{high}}$ group ($-4.59\ \mu V/m^2 \pm 2.39$) and the $\text{rtheta}_{\text{low}}$ group ($-3.02\ \mu V/m^2 \pm 1.90$) did not differ significantly ($t(84) = 0.52$, $p = .607$, $d = -0.11$). Furthermore, we found a significant main effect of the

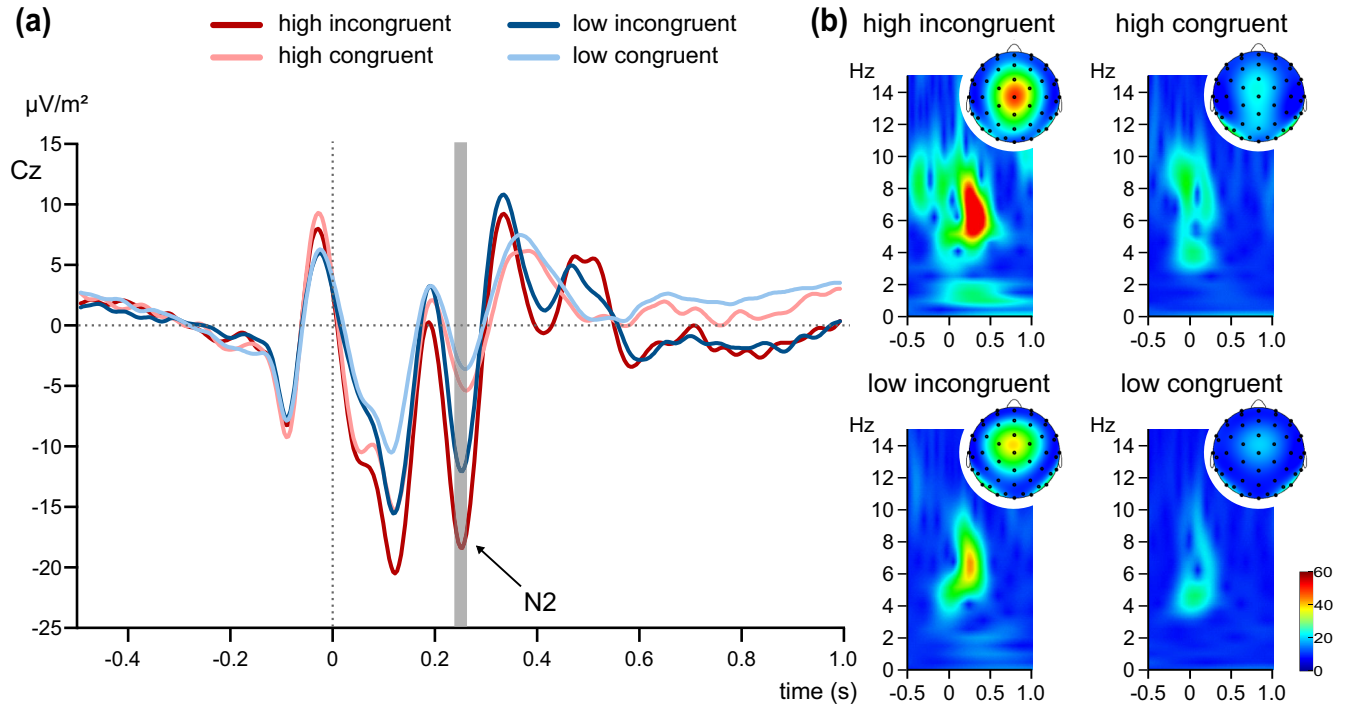

FIGURE 1 Standard event-related potentials (ERPs) and total theta power. The left plot (a) illustrates standard ERPs with the N2 component at electrode Cz during the flanker task. The incongruent condition is shown in dark red for the rtheta$_{high}$ group and in dark blue for the rtheta$_{low}$ group. The congruent condition is illustrated in light red for the rtheta$_{high}$ group and light blue for the rtheta$_{low}$ group. The area marked in gray shows the time range that was used for the statistical analyses. The *x*-axis denotes time in seconds (s) relative to the target stimulus onset; the *y*-axis displays the amplitude of the ERP data in µV/m^2. The right part of the Figure (b) shows the time-frequency decomposition plots for the rtheta$_{high}$ group and the rtheta$_{low}$ group in the incongruent and congruent condition, respectively. The plots represent total theta power at electrode Cz and include the corresponding scalp topographies. The *x*-axis displays time in seconds (s) relative to the target stimulus onset and the *y*-axis denotes frequency in Hertz (Hz). Power is indicated by color

factor *congruency* ($F_{(1,84)}$ = 101.10, p < .001, ηp^2 = .55), with incongruent trials being associated with larger N2 amplitudes (−14.62 µV/m^2 ± 1.63) than congruent trials (−3.81 µV/m^2 ± 1.52). No other main effects or interactions were significant (all F < 1.77, all p > .187).

3.2.2 | Time-frequency analysis of standard ERPs

To analyze group differences of total theta power at electrode Cz in the time window from 100 ms to 400 ms after onset of the target stimulus, we performed a mixed-effects ANOVA. The analysis revealed a significant interaction effect *congruency* × *group* ($F_{(1,84)}$ = 6.63, p = .012, ηp^2 = .07). Posthoc tests showed that the interaction was driven by a *group* difference during incongruent trials (t(84) = −2.88, p = .005, d = 0.62). In the incongruent condition, the rtheta$_{high}$ group showed stronger total theta power (147.13 ± 18.35) than the rtheta$_{low}$ group (89.01 ± 8.35). During congruent trials, no significant difference of total theta power between the rtheta$_{high}$ group (54.94 ± 9.45) and the rtheta$_{low}$ group (35.81 ± 4.38) was evident (t(84) = −1.84, p = .070, d = 0.40). Furthermore, a main effect of *group* ($F_{(1,84)}$ = 7.46, p = .008, ηp^2 = .08), as well as a main effect of *congruency* ($F_{(1,84)}$ = 92.20, p < .001, ηp^2 = .52) was observed. Total theta power was generally higher in the rtheta$_{high}$ group (101.04 ± 13.06) in comparison to the rtheta$_{low}$ group (62.41 ± 5.44). Additionally, incongruent trials were associated with larger total theta power (118.07 ± 10.53) than congruent trials (45.38 ± 5.28). Figure 1b shows total theta power for both groups and both conditions.

3.2.3 | RIDE decomposition

The results of the RIDE decomposition are displayed in Figure 2.

In the S-cluster, the mixed-effects ANOVA revealed a significant interaction of *congruency* × *group* for the N2 at electrode Cz ($F_{(1,84)}$ = 6.02, p = .016, ηp^2 = .07; see Figure 2a). Substantiating the results of the standard ERP analysis, posthoc tests showed a *group* effect in the incongruent condition. During incongruent trials, N2 amplitudes were significantly larger in the rtheta$_{high}$ group (−19.47 µV/m^2 ± 2.2) in comparison to the rtheta$_{low}$ group (−13.49 µV/m^2 ± 1.82, t(84) = 2.09, p = .04, d = −0.45). No significant group differences were evident during compatible trials (rtheta$_{high}$: −5.88 µV/m^2 ± 1.56, rtheta$_{low}$: −4.62 µV/m^2 ± 1.23, t(84) = 0.63, p = .528, d = −0.14). Furthermore, the main effect of *congruency* yielded a significant effect ($F_{(1,84)}$ = 136.10, p < .001, ηp^2 = .62), with incongruent trials involving larger N2 amplitudes (−16.48 µV/m^2 ± 1.46) than congruent trials (−5.25 µV/m^2 ± 0.99). No further

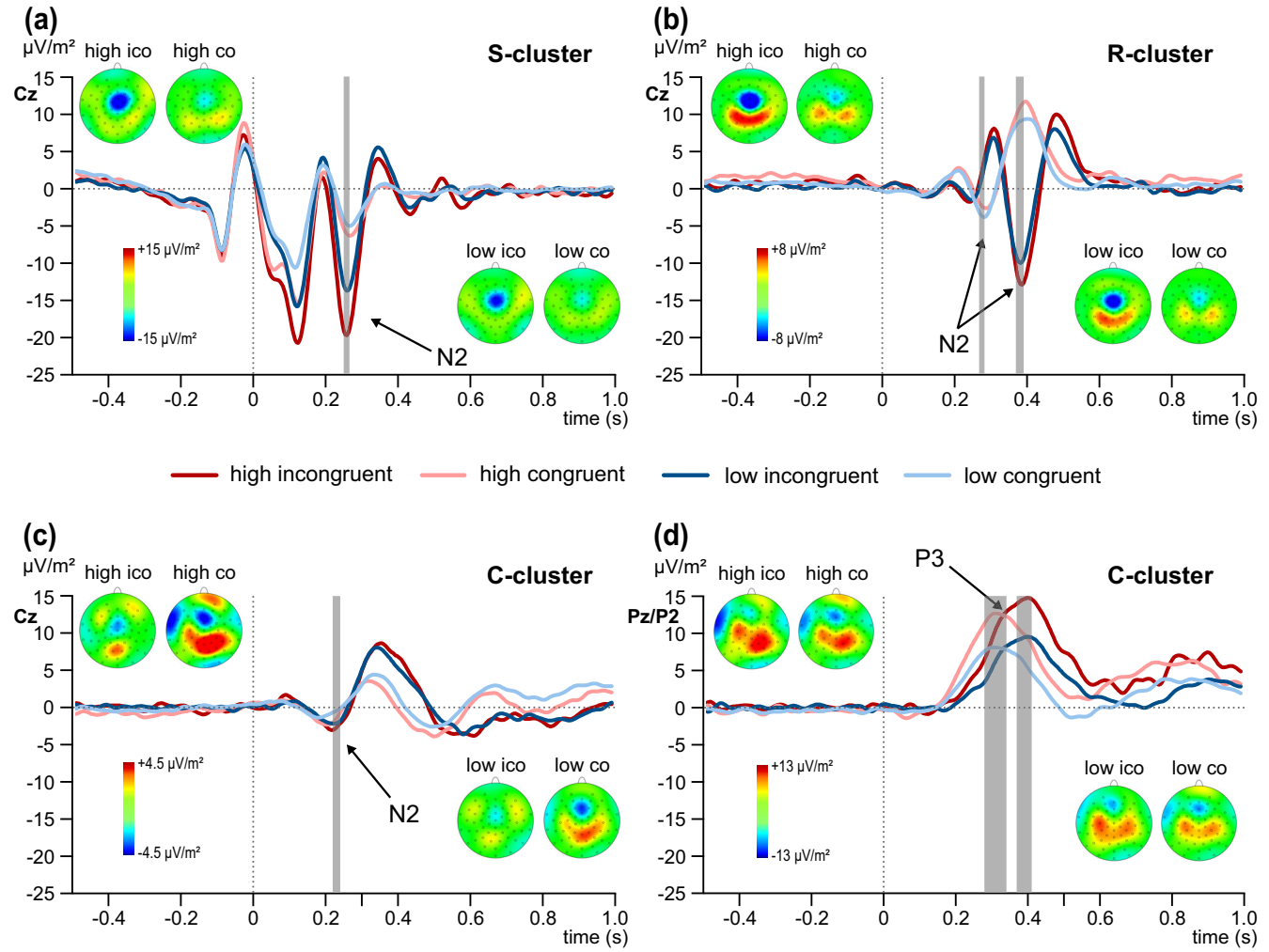

FIGURE 2 Results of the RIDE analysis. The plots show the decomposed event-related potential (ERP) data of the S-cluster at electrode Cz (a), of the R-cluster at electrode Cz (b), of the C-cluster at electrode Cz (c), and of the C-cluster at electrodes Pz/P2 (d) with the corresponding scalp topographies. The incongruent condition (ico) is shown in dark red for the $rtheta_{high}$ group and in dark blue for the $rtheta_{low}$ group. The congruent condition (co) is illustrated in light red for the $rtheta_{high}$ group and light blue for the $rtheta_{low}$ group. The areas marked in gray show the time ranges that were used for the statistical analyses. Due to a latency shift, the peaks of the N2 component in the R-Cluster (b) and of the P3 component in the C-cluster (d) differed for the congruent and incongruent conditions. For this reason, separate analysis windows were quantified for each condition. The *x*-axis denotes time in seconds (s) relative to the target stimulus onset; the *y*-axis displays the amplitudes of the ERP data in $\mu V/m^2$. The scalp topographies show the potential distribution at the peak of the corresponding RIDE cluster components (a–c: N2 component, d: P3 component). Blue colors denote negative potentials; red colors denote positive potentials

interaction or main effects were evident (all $F < 3.72$, all $p > .057$). To rule out that the unequal number of trials in the congruent vs. incongruent condition affected the results, we repeated this analysis with a subsample with equal numbers of trials in both conditions (see Supporting Information S1).

In the C-cluster, only a main effect of *congruency* was evident at electrode Cz in the N2 time window ($F_{(1,84)} = 4.01$, $p = .049$, $\eta p^2 = .05$; see Figure 2c). During incongruent trials, N2 amplitude was larger (–2.44 $\mu V/m^2 \pm 0.51$) than during congruent trials (–1.04 $\mu V/m^2 \pm 0.75$). All other main effects or interactions at electrodes Cz and FCz were not significant (all $F < 1.76$, all $p > .189$). To substantiate the lack of a significant *congruency* × *group* interaction effect, we performed Bayesian analysis (Masson, 2011) to calculate the probability of the null hypothesis being true given the obtained data $p(H_0/D)$. For the interaction of *congruency* × *group*, Bayesian analysis revealed $p(H_0/D) = 0.90$. According to Raftery (Raftery, 1995), this shows that there is positive evidence in favor of the null hypothesis.

In the C-cluster, we additionally analyzed the prominent P3-like positivity at electrodes Pz and P2 (see Figure 2d), since P3-like activity is most commonly reflected by this cluster (Ouyang, Hildebrandt, Sommer, & Zhou, 2017). The mixed-effects ANOVA revealed a main effect of *group* ($F_{(1,84)} = 6.31$, $p = .014$, $\eta p^2 = .07$) with larger amplitudes in the $rtheta_{high}$ group (13.46 $\mu V/m^2 \pm 1.48$) than in the $rtheta_{low}$ group (8.69 $\mu V/m^2 \pm 1.19$). Furthermore, incongruent trials revealed larger amplitudes in this P3 time window (11.95 $\mu V/m^2 \pm 1.14$) than congruent trials (10.20 $\mu V/m^2 \pm 0.93$, $F_{(1,84)} = 6.16$, $p = .015$, $\eta p^2 = .07$). No further main effects and interactions yielded significant results (all $F < 0.50$, all $p > .484$).

Finally, we analyzed the R-cluster at electrode Cz in the N2 time window (see Figure 2b). Like in both other clusters, a significant main effect of *congruency* was evident ($F_{(1,84)}$ = 43.67, p < .001, ηp^2 = .34), with larger N2 amplitudes in incongruent trials (−10.93 μV/m^2 ± 1.47) than in congruent trials (−2.91 μV/m^2 ± 0.82). No further main effects or interactions were significant (all F < 2.48, all p > .119). Again, we corroborated the lack of a significant interaction *congruency* × *group* with Bayes statistics. The analysis revealed $p(H_0/D)$ = 0.73, providing weak evidence (but close to the cut-off value of 0.75 for positive evidence) for the null hypothesis being true.

3.2.4 | Time-frequency analysis of RIDE data

Since the RIDE decomposition only revealed an interaction *congruency* × *group* in the S-cluster, a wavelet analysis to examine the total theta power was specifically performed for the S-cluster. As with the standard ERP data, we analyzed total theta power at electrode Cz in the time window between 100 and 400 ms after the target stimulus onset. Figure 3a shows total theta power for both groups (rtheta$_{high}$ and rtheta$_{low}$) and both conditions (congruent and incongruent).

The mixed effects ANOVA revealed a significant interaction *congruency* × *group* ($F_{(1,84)}$ = 7.20, p = .009, ηp^2 = .08). Posthoc tests showed that a group effect was evident in the congruent (t(84)= −2.31, p = .023, d = 0.50), as well as in the incongruent condition (t(84)= −2.98, p = .004, d = 0.64). In both conditions, the rtheta$_{high}$ group was characterized by higher total theta power (congruent: 52.68 ± 8.58, incongruent: 138.62 ± 17.83) than the rtheta$_{low}$ group (congruent: 31.13 ± 3.66, incongruent: 80.98 ± 7.43). However, effect sizes indicate that the interaction effect was driven by the group differences during incongruent trials. The beamforming analysis revealed that the difference of total theta power between the rtheta$_{high}$ group and the rtheta$_{low}$ group during incongruent trials is associated with activation differences in the supplementary motor area (SMA), the middle occipital region and the right triangular/opercular part of the inferior frontal gyrus (IFG, see Figure 3b). In addition to the interaction effect, a significant main effect of the factor *group* corroborated the finding that the rtheta$_{high}$ group showed generally stronger total theta

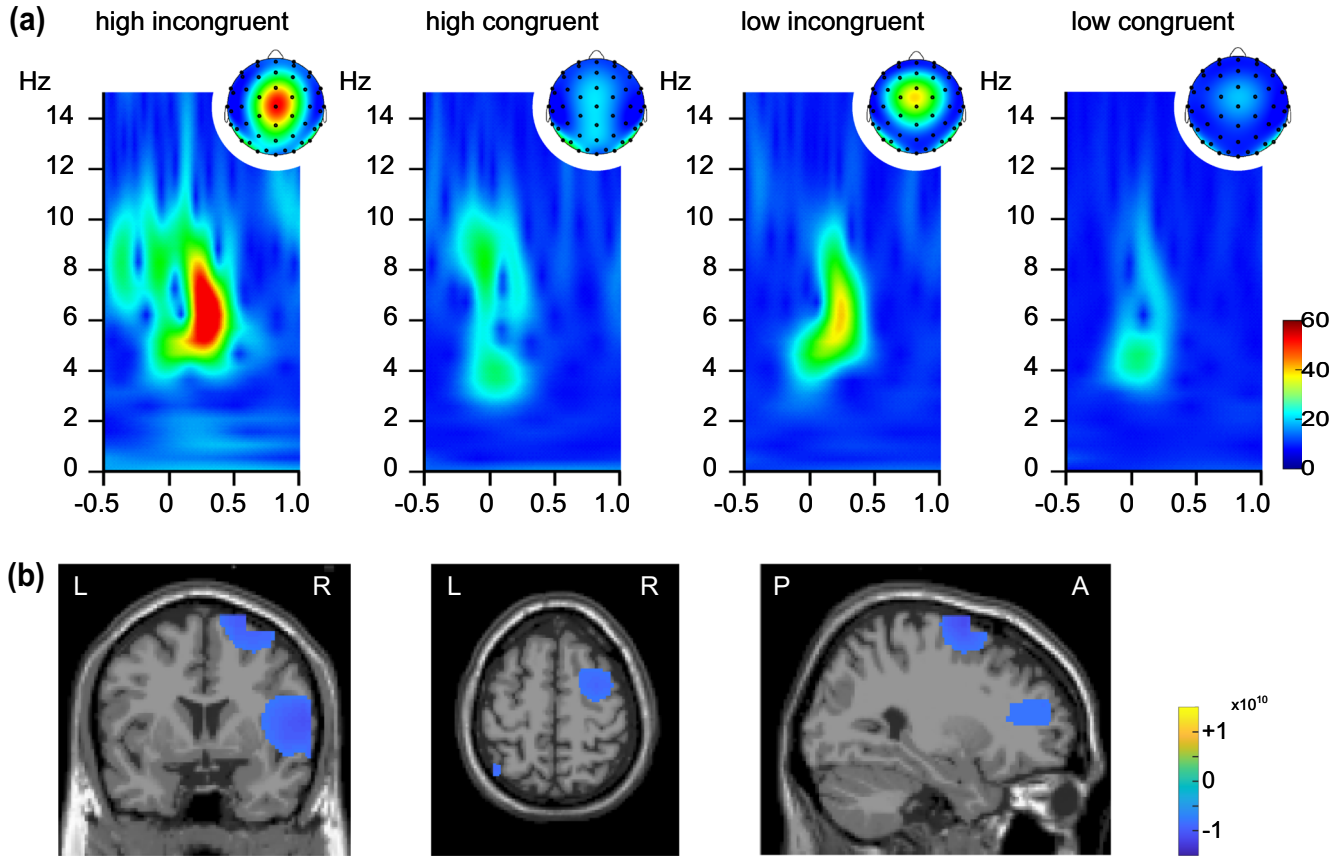

FIGURE 3 Total theta power of the RIDE S-cluster and beamforming analysis. Part (a) of the figure shows the time-frequency decomposed plots for the rtheta$_{high}$ group and the rtheta$_{low}$ group in both, incongruent and congruent conditions. The plots represent the total theta power at electrode Cz in the S-cluster and include the corresponding scalp topographies. The *x*-axis displays time in seconds (s) relative to the target stimulus onset and the *y*-axis denotes frequency in Hertz (Hz). Power is indicated by color. Part (b) shows the results of the beamforming analysis contrasting total theta power of the rtheta$_{high}$ group with total theta power of the rtheta$_{low}$ group during incongruent trials. The difference in total theta power is associated with activation differences in the supplementary motor area (SMA), the inferior frontal gyrus (IFG) and the middle occipital gyrus

power (95.65 ± 12.75) than the $rtheta_{low}$ group (56.06 ± 4.73, ($F_{(1,84)}$ = 8.48, p = .005, ηp^2 = .09). Moreover, in incongruent trials, total theta power was higher (109.80 ± 10.10) than in congruent trials (41.91 ± 4.78, ($F_{(1,84)}$ = 101.87, p < .001, ηp^2 = .08).

3.2.5 | Correlation analyses

To analyze the relationship between resting theta activity and conflict monitoring in more detail, we additionally performed correlation analyses between resting theta activity and the task-related behavioral and neurophysiological variables. We used the false discovery rate approach to correct for multiple testing (Benjamini & Hochberg, 1995). For the standard ERP data, the correlation analyses showed no significant correlation between resting theta activity and the N2 amplitude at electrode Cz in the congruent condition (r(84) = −.20, p = .085, 95% CI [−.42, .07]). In the incongruent condition, however, there was a significant negative correlation (r(84) = −.27, p = .018, [−.46, −.06]). A higher level of resting theta activity was associated with a larger N2 amplitude. A Bayesian correlation analysis substantiated these results by providing only anecdotal evidence for a correlation between resting theta and the N2 amplitude in the congruent condition (Bayes Factor (BF) = 0.65) but moderate evidence for the correlation in the incongruent condition (BF = 3.87). Furthermore, a positive correlation between resting theta activity and total theta power at electrode Cz was revealed in the congruent (r(84) = .33, p = .006, [.10, .49]), as well as in the incongruent condition (r(84) = .43, p = .004, [.25, .57]). After the signal decomposition, the correlation analyses showed similar results for the N2 amplitude at electrode Cz in the S-cluster as before for the standard N2: during the congruent trials, there was no significant correlation between resting theta and the N2 amplitude in the S-cluster evident (r(84) = −.20, p = .086, [−.41, .06]). During incongruent trials, however, the data revealed a negative association between resting theta activity and the N2 amplitude (r(84) = −.27, p = .018, [−.46, −.07]). Again, the Bayesian correlation analysis corroborated these results. The evidence for a correlation between resting theta activity and the N2 amplitude in the S-cluster was anecdotal for the congruent condition (BF = 0.79) but moderate for the incongruent condition (BF = 4.97). As with the standard ERP data, positive correlations between resting theta activity and total theta power in the congruent condition (r(84) = .37, p = .004, [.19, .52]) and in the incongruent condition (r(84) = .47, p = .004, [.33, .60]) were evident at electrode Cz in the S-cluster. In the R-cluster, the correlations between the resting theta activity and the N2 amplitude at electrode Cz were neither significant in the congruent condition (r(84) = −.03, p = .793, [−.25, .17]) nor in the incongruent condition (r(84) = −.12, p = .277, [−.32, .07]). Resting theta activity was positively correlated with the P3 amplitude at electrodes Pz/P2 in the C-cluster, both during congruent trials ((r(84) = .27, p = .018, [.03, .47]) and incongruent trials ((r(84) = .28, p = .018, [.03, .47]). Figure 4 shows the scatterplots of main interest (correlation between resting theta activity and N2-amplitude (Figure 4a)/total theta power (Figure 4b) in the standard ERP during incongruent trials; correlation between resting theta activity and N2-amplitude (Figure 4c) / total theta power (Figure 4d) in the S-cluster during the incongruent trials).

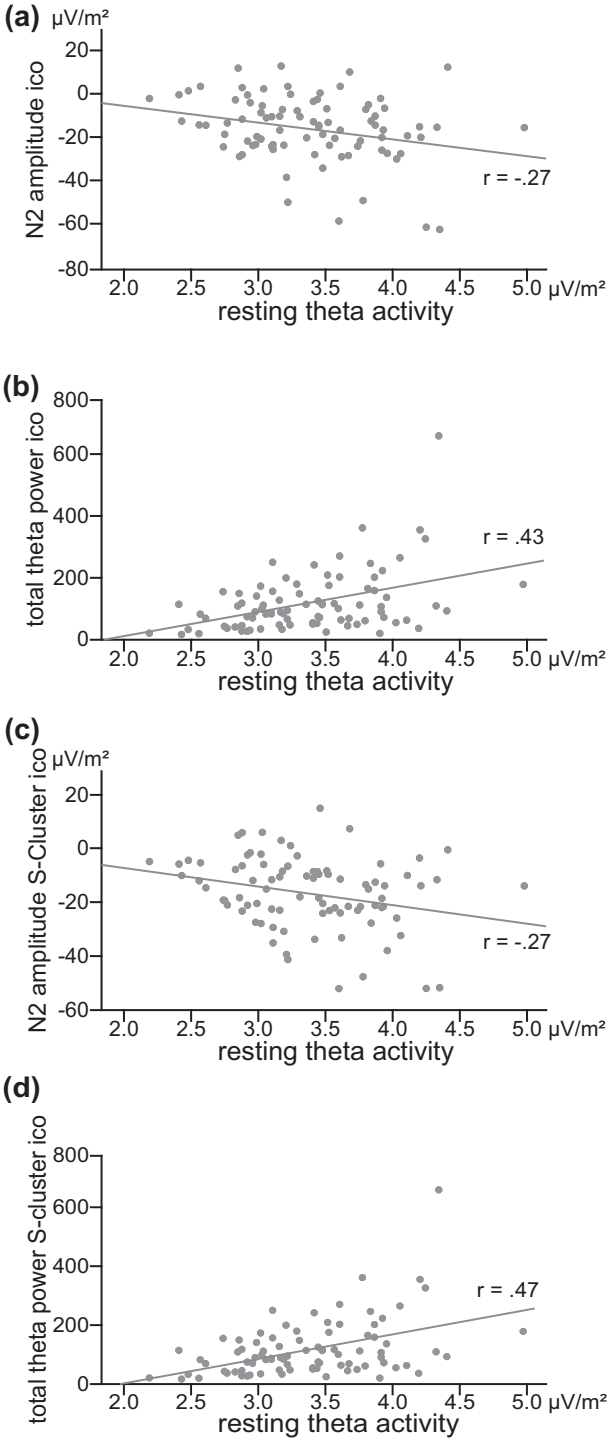

FIGURE 4 Scatterplots. The plots a–d illustrate the correlation between resting theta activity in μV/m² (x-axis) and several neurophysiological outcome variables during the incongruent flanker condition (ico, y-axis). The following variables are shown at the y-axes of plots a–d: standard event-related potential (ERP) N2 amplitude at electrode Cz in μV/m² (a), total theta power of the standard ERP data at electrode Cz (b), N2 amplitude in the RIDE S-cluster at electrode Cz in μV/m² (c) and total theta power of the RIDE S-cluster at electrode Cz (d)

The focus of this study is primarily the understanding of the neurophysiological processes underlying conflict monitoring. Nevertheless, we correlated the decomposed neurophysiological data with the participants' task performance to provide a full picture of the data. Again, we used the false discovery rate approach to correct for multiple testing (Benjamini & Hochberg, 1995). The analyses revealed a significantly positive correlation between the P3 amplitude in the C-cluster at electrodes Pz/P2 in the incongruent condition and the hit rate during incongruent trials ($r(84) = .33$, $p = .032$, [.17, .46]) but no significant correlation with the reaction time during incongruent trials ($r(84) = -.25$, $p = .152$, [−.49, .01]). In the congruent condition, there were no significant correlations with the hit rate ($r(84) = .06$, $p = .922$, [−.10, .21]) and the reaction time ($r(84) = .02$, $p = .922$, [−.17, .19]) evident. The N2 amplitude in the S-cluster and in the R-cluster and the event-related total theta power in the S-cluster did also not correlate significantly with the participants' task performance (all corrected $p > .272$). To substantiate these lacks of correlation between the neurophysiological data in the S- and R-cluster and the task performance, we again calculated Bayesian correlation analyses. For all analyses the results revealed anecdotal to moderate evidence for the null hypothesis, that is, the probability that no significant correlation exists is clearly higher than the probability that a significant correlation exists (all BF between 0.13 and 0.87).

4 | DISCUSSION

In the current study, we examined the strength of the association between resting theta band activity and conflict-related neurophysiological activity. In a previous study, we have already shown that resting theta activity is related to task-related theta activity during motor response inhibition (Pscherer et al., 2019). Unlike these previous data (Pscherer et al., 2019), we here focus on conflict monitoring (or interference control), which is different from motor inhibition processes, even though some inhibitory control aspect has also been discussed for the control of conflicting sensory information (Chmielewski, Mückschel, Roessner, & Beste, 2014; Klein, Petitjean, Olivier, & Duque, 2014; Ocklenburg, Güntürkün, & Beste, 2011; Stürmer, Siggelkow, Dengler, & Leuthold, 2000; Tandonnet, Garry, & Summers, 2011; Verleger, Kuniecki, Möller, Fritzmannova, & Siebner, 2009). Moreover, the specific focus of this study was to examine whether distinct information coding levels during conflict monitoring processes are differentially affected by the strength of resting theta band activity. Thus, these data not only show whether there are associations between resting state and conflict-related neural activity, but also whether such associations are specific for the information being coded during conflict monitoring. The data suggest that this is indeed the case.

For the standard ERP data (i.e., N2), the results revealed that the amplitude of the N2 was larger in the group showing relatively high resting theta power ($rtheta_{high}$), compared to the group showing relatively low resting theta power ($rtheta_{low}$) in conflicting, that is, incongruent trials. In nonconflicting trials, no group difference was evident. The same interactive pattern between group and trial compatibility was shown when analyzing total theta power (consisting of phase-locked and nonphase-locked aspects of theta power). Here, the $rtheta_{high}$ group was also characterized by higher theta band power in conflicting trials than the $rtheta_{low}$ group. This suggests a direct link between resting state theta activity and conflict-related theta activity. Together with previous findings reporting a link between resting state and task-related theta activity in an inhibition task (Pscherer et al., 2019), this study provides further indications for the assumption that resting theta activity may be related to cognitive control-related processes. The revealed link was further substantiated by the results of the correlation analyses which showed for higher resting theta activity to be associated with larger N2 amplitudes during incongruent trials, but not during congruent trials. The task-related theta activity, however, was correlated with resting theta activity in both conditions. The results imply that there is a general relationship between resting and task-related theta activity, which is even more intense during conflict monitoring processes.

Until now only task-related theta activity was investigated in the context of signal decomposition. The current study is the first to demonstrate a relationship between resting theta activity and the decomposed EEG signal. The important novel finding is that resting state activity in the theta frequency band is very specifically associated with dissociable neuronal subprocesses (information coding levels) involved in conflict monitoring. The data showed a clear dissociation between the association of resting theta band activity with the S-cluster data and the association with activity in the other two clusters. For the S-cluster data, the same interactive pattern as obtained for the standard ERP data was evident. Again, the amplitude in the N2 time window was larger (more negative) in the $rtheta_{high}$ group than in the $rtheta_{low}$ group in conflicting trials. No group effects were observed for nonconflicting trials. The analysis of the total theta power in the N2 time range of the S-cluster corroborated this pattern of results with group differences in total theta power around 6.5 Hz during conflicting trials. As with the standard ERP data, correlation analyses revealed that a higher resting theta power was associated with larger N2 amplitudes and stronger total theta power during incongruent trials in the S-cluster. During congruent trials, resting theta activity was only correlated with task-related total theta power, not with the N2 amplitude. Beamforming data showed that the differences of event-related total theta power between $rtheta_{high}$ group and $rtheta_{low}$ group in the incongruent condition were due to activation differences in the medial parts of the superior frontal gyrus (BA6), also encompassing the supplemental motor area (SMA), as well as in the right inferior frontal gyrus (BA 44/45) and the middle occipital gyrus. Previous data already suggested that stimulus-related, medial frontal theta activity is coded in the upper theta frequency band (around 6.5–7 Hz; Mückschel, Dippel, & Beste, 2017). This converging evidence lends further support to the assumption that there are distinct stimulus and response selection codes in theta frequency band during cognitive control processes (Mückschel, Dippel, & Beste, 2017). Notably, however, the R-cluster and the C-cluster did not reveal interactive effects between group and trial compatibility.

This was substantiated by a Bayesian analysis of the data which revealed positive evidence in favor of the null hypothesis for the C-cluster and weak (but close to positive) evidence in favor of the null hypothesis for the R-cluster. Furthermore, in the R-cluster, we observed no significant correlations between resting theta activity and the task-related variables. In the C-cluster, resting theta activity was correlated positively with the amplitude of the P3 component in both conditions. Since the P3 component is commonly not associated with activity in the theta frequency band, but with slower brain wave activity, and since the correlations were not specific for the conflict condition, this result implies that resting theta activity could also be related to task-related processes, which are communicated through brain activity in different frequency ranges. With regard to conflict monitoring, however, resting theta band activity seems to be specifically associated with the processing of stimulus-related aspects. It seems that resting state theta activity is only relevant for some subprocesses during conflict monitoring and does not have a cross-coding level relevance for conflict monitoring mechanisms. This further specifies the relevance of nonphase-locked (combined with phase-locked) activity during conflict monitoring. However, why should especially stimulus-related processes be this important during conflict monitoring and how may this explain why resting theta activity is associated with stimulus-related theta activity during conflict monitoring?

Previous findings already showed that stimulus-coding aspects involved in conflict monitoring and reflected in the N2 time window are quite specifically reflected by activity in the theta frequency band (Mückschel, Dippel, & Beste, 2017). Interestingly, it has been suggested that EEG theta oscillations during conflict tasks may not reflect conflict monitoring per se, but the *input integration* processes that lead to the detection of conflict (Cohen, 2014). This suggestion is based on considerations that EEG conflict theta activity represents oscillations in superficial cortical Layers 2 and 3 (Cohen, 2014; Wang, Ulbert, Schomer, Marinkovic, & Halgren, 2005), which yield a cellular architecture ideally suited to filter, amplify and integrate information (Douglas & Martin, 2004; Mel, 1993). The beamforming analysis, conducted for the current data, showed that the increase of theta power during conflicting trials in the $\text{rtheta}_{\text{high}}$ group compared to the $\text{rtheta}_{\text{low}}$ group was associated with activation differences particularly in the superior frontal gyrus (SFG, BA6), encompassing the SMA, as well as in the right inferior frontal gyrus (BA 44/45). This is in line with several previous studies on the functional neuroanatomy of conflict monitoring (Herz et al., 2014; Mars et al., 2009; Mückschel et al., 2016; Nachev et al., 2008; Rushworth et al., 2004; Stock et al., 2013). These findings show that especially medial frontal areas are affected by perceptual modulations of cognitive control (Labrenz, Themann, Wascher, Beste, & Pfleiderer, 2012; Westerhausen et al., 2010). This is also in line with other data suggesting that these regions are involved in sensory evidence integration (Tosun, Berkay, Sack, Çakmak, & Balcı, 2017). Since conflict control is (partly) achieved by inhibitory control processes acting on the conflicting information (Chmielewski et al., 2014; Klein et al., 2014; Ocklenburg et al., 2011; Stürmer et al., 2000; Verleger et al., 2009), the involvement of the rIFG as an important hub in the cortical inhibitory control network (Bari & Robbins, 2013) seems also reasonable and has already been reported to be involved in conflict monitoring (Bensmann, Roessner, Stock, & Beste, 2018). More recent data on the modulation of S-cluster activity in the N2 time window and the theta frequency range in particular further supports the SFG-finding (Mückschel, Chmielewski, et al., 2017; Mückschel, Dippel, & Beste, 2017). Even more importantly, these superior frontal regions show close structural neuroanatomical connections to visual association areas (Hagmann et al., 2008). This is a prerequisite for the integration of inputs in an efficient way. Together, these considerations can explain the outstanding role of stimulus-related processes during conflict monitoring, but they cannot explain why resting theta power is specifically related to total theta power during conflict monitoring. Previous findings suggest that similarities or overlaps in neural networks implicated in resting activity and task-related activity may be one reason why specific resting state dynamics are closely related to task-related neural activity (Becker et al., 2018; Tavor et al., 2016). Indeed, evidence from intra-cerebral recordings in humans and monkeys (Tsujimoto, Shimazu, & Isomura, 2006; Tsujimoto, Shimazu, Isomura, & Sasaki, 2010; Wang et al., 2005), as well as from in vitro cell preparations from the medial frontal cortex (van Aerde et al., 2009) reveals that cortical structures involved in cognitive control-related theta band activity also produce endogenous theta band activity (Cohen, 2014). In this respect, strongly overlapping areas are likely involved in the generation of theta signals at rest and during cognitive control (conflict monitoring). Exactly this overlap could be the reason why resting state theta band power has an effect on phase-locked and nonphase-locked theta band activity during conflict monitoring and the previously investigated motor response inhibition.

Nevertheless, we cannot rule out that the observed effects may not be specifically due to differences in the resting theta level. There may exist potentially confounding effects that affect the reported results. For example, a higher resting theta level might also be associated with other factors such as higher motivation, better attention or a higher resting level in other frequency bands. A limiting factor in our study is that we prefiltered the data online (see Section 2.2) and thus did not record data of other frequency bands in the resting state. Thus, we were not able to examine the relationship between the resting state activity of other frequency bands and the task-related EEG and time-frequency activity. Therefore, we cannot exclude the possibility that the effects we found are due to general activation differences in the resting EEG and not specifically to differences in the resting theta activity. A differentiated analysis of possible confounding factors and other frequency bands in the resting state should be addressed in future research.

It needs to be noted that there were no interactive effects between group and trial compatibility at the behavioral level. Even though we found general effects of trial compatibility (i.e., error rates and reaction times increased in conflicting trials), the groups did not differ in their behavior in conflicting and nonconflicting trials. The reason for this may be related to the observed specificity of group effects at the neurophysiological level. As mentioned, only stimulus-related processes during conflict monitoring were associated with the level of

resting theta activity, but not motor response-related and decision-related processes. The processes presumably reflecting stimulus–response transition and decision-making were, however, the only aspect of the decomposed EEG signal, which was related to the task performance during incongruent trials. Our findings imply that the level of resting theta activity is associated with the stimulus processing which in turn is not necessarily or exclusively linked to the task performance. Other factors seem to impact the decision-related processes, which explain the variation in conflict monitoring on a behavioral level. Indeed, in previous studies, which did show effects on the behavioral level, not only modulations of stimulus-related processes were observed but also modulations of motor response-related and/or decision-related processes (Mückschel, Chmielewski, et al., 2017; Mückschel, Dippel, & Beste, 2017). As outlined, theta activity during conflict tasks may not reflect conflict monitoring per se, but the input integration process leading to the detection of conflict (Cohen, 2014). This may be the reason why the observed modulations were present at the neurophysiological level and absent at the behavioral level. On the other hand, it is possible that subjects with a lower resting theta level may be able to compensate for this "deficit" by other factors (e.g., faster reaction selection, etc.) and thus reach a similar performance level.

5 | CONCLUSIONS

In summary, we showed that resting state theta activity is closely associated with the strength of conflict-related neural activity at the level of ERPs and total theta power. The important new finding of the data is that resting state theta activity is only associated with a specific aspect of conflict-related theta activity in superior and inferior frontal regions and the supplemental motor area (SMA, BA6) in particular. Only stimulus-related coding levels, but not motor response related coding levels, during nonphase locked theta activity were associated with resting theta activity. This specificity of effects may explain why resting state theta activity may not affect overt behavioral performance during cognitive control. The results suggest that resting state theta activity is particularly important to consider for input integration processes during cognitive control.

ACKNOWLEDGMENTS

This work was supported by grants from the Deutsche Forschungsgemeinschaft (DFG) SFB 940 project B8 and partly by the Collaborative Research Center/Transregio (TRR 265) project B7. Open access funding enabled and organized by Projekt DEAL.

[Correction added on November 17, 2020, after first online publication: Projekt Deal funding statement has been added.]

CONFLICT OF INTEREST

The authors declare no conflict of interest.

DATA AVAILABILITY STATEMENT

The data that support the findings of this study are available from the corresponding author upon reasonable request.

ORCID

Moritz Mückschel https://orcid.org/0000-0002-9069-7803

Christian Beste https://orcid.org/0000-0002-2989-9561

REFERENCES

Bari, A., & Robbins, T. W. (2013). Inhibition and impulsivity: Behavioral and neural basis of response control. *Progress in Neurobiology*, *108*, 44–79.

Becker, R., Van de Ville, D., & Kleinschmidt, A. (2018). Alpha oscillations reduce temporal long-range dependence in spontaneous human brain activity. *The Journal of Neuroscience*, *38*, 755–764.

Benjamini, Y., & Hochberg, Y. (1995). Controlling the false discovery rate: A practical and powerful approach to multiple testing. *Journal of the Royal Statistical Society Series B (Methodological)*, *57*, 289–300.

Bensmann, W., Roessner, V., Stock, A.-K., & Beste, C. (2018). Catecholaminergic modulation of conflict control depends on the source of conflicts. *The International Journal of Neuropsychopharmacology*, *21*, 901–909.

Botvinick, M. M., Braver, T. S., Barch, D. M., Carter, C. S., & Cohen, J. D. (2001). Conflict monitoring and cognitive control. *Psychological Review*, *108*, 624–652.

Botvinick, M. M., & Cohen, J. D. (2014). The computational and neural basis of cognitive control: Charted territory and new frontiers. *Cognitive Science*, *38*, 1249–1285.

Buzsáki, G., & Draguhn, A. (2004). Neuronal oscillations in cortical networks. *Science*, *304*, 1926–1929.

Cavanagh, J. F., & Frank, M. J. (2014). Frontal theta as a mechanism for cognitive control. *Trends in Cognitive Sciences*, *18*, 414–421.

Cavanagh, J. F., Zambrano-Vazquez, L., & Allen, J. J. B. (2012). Theta lingua franca: A common mid-frontal substrate for action monitoring processes. *Psychophysiology*, *49*, 220–238.

Chmielewski, W. X., Mückschel, M., Roessner, V., & Beste, C. (2014). Expectancy effects during response selection modulate attentional selection and inhibitory control networks. *Behavioural Brain Research*, *274*, 53–61.

Cohen, M. X. (2014). A neural microcircuit for cognitive conflict detection and signaling. *Trends in Neurosciences*, *37*, 480–490.

De Blasio, F. M., & Barry, R. J. (2013). Prestimulus delta and theta determinants of ERP responses in the go/NoGo task. *International Journal of Psychophysiology*, *87*, 279–288.

Dippel, G., Mückschel, M., Ziemssen, T., & Beste, C. (2017). Demands on response inhibition processes determine modulations of theta band activity in superior frontal areas and correlations with pupillometry - Implications for the norepinephrine system during inhibitory control. *NeuroImage*, *157*, 575–585.

Douglas, R. J., & Martin, K. A. C. (2004). Neuronal circuits of the neocortex. *Annual Review of Neuroscience*, *27*, 419–451.

Faul, F., Erdfelder, E., Lang, A.-G., & Buchner, A. (2007). G*Power 3: A flexible statistical power analysis program for the social, behavioral, and biomedical sciences. *Behavior Research Methods*, *39*, 175–191.

Folstein, J. R., & Van Petten, C. (2008). Influence of cognitive control and mismatch on the N2 component of the ERP: A review. *Psychophysiology*, *45*, 152–170.

Gross, J., Kujala, J., Hamalainen, M., Timmermann, L., Schnitzler, A., & Salmelin, R. (2001). Dynamic imaging of coherent sources: Studying neural interactions in the human brain. *Proceedings of the National Academy of Sciences of the United States of America*, *98*, 694–699.

Hagmann, P., Cammoun, L., Gigandet, X., Meuli, R., Honey, C. J., Wedeen, V. J., & Sporns, O. (2008). Mapping the structural Core of human cerebral cortex. *PLoS Biology*, *6*, e159.

Harper, J., Malone, S. M., & Bernat, E. M. (2014). Theta and delta band activity explain N2 and P3 ERP component activity in a go/no-go task. *Clinical Neurophysiology*, *125*, 124–132.

Herz, D. M., Christensen, M. S., Bruggemann, N., Hulme, O. J., Ridderinkhof, K. R., Madsen, K. H., & Siebner, H. R. (2014).

Motivational tuning of fronto-subthalamic connectivity facilitates control of action impulses. *The Journal of Neuroscience*, *34*, 3210–3217.

Hiltunen, T., Kantola, J., Abou Elseoud, A., Lepola, P., Suominen, K., Starck, T., … Palva, J. M. (2014). Infra-slow EEG fluctuations are correlated with resting-state network dynamics in fMRI. *The Journal of Neuroscience*, *34*, 356–362.

Huster, R. J., Plis, S. M., & Calhoun, V. D. (2015). Group-level component analyses of EEG: Validation and evaluation. *Frontiers in Neuroscience*, *9*, 254.

Klein, P.-A., Petitjean, C., Olivier, E., & Duque, J. (2014). Top-down suppression of incompatible motor activations during response selection under conflict. *NeuroImage*, *86*, 138–149.

Knyazev, G. G. (2013). EEG correlates of self-referential processing. *Frontiers in Human Neuroscience*, *7*, 264. http://journal.frontiersin.org/article/10.3389/fnhum.2013.00264/abstract

Labrenz, F., Themann, M., Wascher, E., Beste, C., & Pfleiderer, B. (2012). Neural correlates of individual performance differences in resolving perceptual conflict. *PLoS One*, *7*, e42849.

Larson, M. J., Clayson, P. E., & Clawson, A. (2014). Making sense of all the conflict: A theoretical review and critique of conflict-related ERPs. *International Journal of Psychophysiology*, *93*, 283–297.

Laufs, H. (2008). Endogenous brain oscillations and related networks detected by surface EEG-combined fMRI. *Human Brain Mapping*, *29*, 762–769.

Love, J., Selker, R., Marsman, M., Jamil, T., Dropmann, D., Verhagen, J., … Epskamp, S. (2019). JASP: Graphical statistical software for common statistical designs. *Journal of Statistical Software*, *88*.

Mars, R. B., Klein, M. C., Neubert, F.-X., Olivier, E., Buch, E. R., Boorman, E. D., & Rushworth, M. F. S. (2009). Short-latency influence of medial frontal cortex on primary motor cortex during action selection under conflict. *The Journal of Neuroscience*, *29*, 6926–6931.

Masson, M. E. J. (2011). A tutorial on a practical Bayesian alternative to null-hypothesis significance testing. *Behavior Research Methods*, *43*, 679–690.

Mel, B. W. (1993). Synaptic integration in an excitable dendritic tree. *Journal of Neurophysiology*, *70*, 1086–1101.

Miller, E. K., & Cohen, J. D. (2001). An integrative theory of prefrontal cortex function. *Annual Review of Neuroscience*, *24*, 167–202.

Mückschel, M., Chmielewski, W., Ziemssen, T., & Beste, C. (2017). The norepinephrine system shows information-content specific properties during cognitive control - Evidence from EEG and pupillary responses. *NeuroImage*, *149*, 44–52.

Mückschel, M., Dippel, G., & Beste, C. (2017). Distinguishing stimulus and response codes in theta oscillations in prefrontal areas during inhibitory control of automated responses. *Human Brain Mapping*, *38*, 5681–5690.

Mückschel, M., Stock, A.-K., Dippel, G., Chmielewski, W., & Beste, C. (2016). Interacting sources of interference during sensorimotor integration processes. *NeuroImage*, *125*, 342–349.

Nachev, P., Kennard, C., & Husain, M. (2008). Functional role of the supplementary and pre-supplementary motor areas. *Nature Reviews. Neuroscience*, *9*, 856–869.

Nakao, T., Bai, Y., Nashiwa, H., & Northoff, G. (2013). Resting-state EEG power predicts conflict-related brain activity in internally guided but not in externally guided decision-making. *NeuroImage*, *66*, 9–21.

Nigbur, R., Cohen, M. X., Ridderinkhof, K. R., & Stürmer, B. (2012). Theta dynamics reveal domain-specific control over stimulus and response conflict. *Journal of Cognitive Neuroscience*, *24*, 1264–1274.

Nunez, P. L., & Pilgreen, K. L. (1991). The spline-Laplacian in clinical neurophysiology: A method to improve EEG spatial resolution. *Journal of Clinical Neurophysiology*, *8*, 397–413.

Nunez, P. L., Srinivasan, R., Westdorp, A. F., Wijesinghe, R. S., Tucker, D. M., Silberstein, R. B., & Cadusch, P. J. (1997). EEG coherency. I: Statistics, reference electrode, volume conduction, Laplacians, cortical imaging, and interpretation at multiple scales. *Electroencephalography and Clinical Neurophysiology*, *103*, 499–515.

Ocklenburg, S., Güntürkün, O., & Beste, C. (2011). Lateralized neural mechanisms underlying the modulation of response inhibition processes. *NeuroImage*, *55*, 1771–1778.

Oostenveld, R., Fries, P., Maris, E., & Schoffelen, J.-M. (2010). FieldTrip: Open source software for advanced analysis of MEG, EEG, and invasive electrophysiological data. *Computational Intelligence and Neuroscience*, *2011*, e156869.

Oostenveld, R., Stegeman, D. F., Praamstra, P., & van Oosterom, A. (2003). Brain symmetry and topographic analysis of lateralized event-related potentials. *Clinical Neurophysiology*, *114*, 1194–1202.

Ouyang, G., Herzmann, G., Zhou, C., & Sommer, W. (2011). Residue iteration decomposition (RIDE): A new method to separate ERP components on the basis of latency variability in single trials. *Psychophysiology*, *48*, 1631–1647.

Ouyang, G., Hildebrandt, A., Sommer, W., & Zhou, C. (2017). Exploiting the intra-subject latency variability from single-trial event-related potentials in the P3 time range: A review and comparative evaluation of methods. *Neuroscience and Biobehavioral Reviews*, *75*, 1–21.

Ouyang, G., Sommer, W., & Zhou, C. (2015). A toolbox for residue iteration decomposition (RIDE)—A method for the decomposition, reconstruction, and single trial analysis of event related potentials. *Journal of Neuroscience Methods*, *250*, 7–21.

Pastötter, B., Dreisbach, G., & Bäuml, K.-H. T. (2013). Dynamic adjustments of cognitive control: Oscillatory correlates of the conflict adaptation effect. *Journal of Cognitive Neuroscience*, *25*, 2167–2178.

Pscherer, C., Mückschel, M., Summerer, L., Bluschke, A., & Beste, C. (2019). On the relevance of EEG resting theta activity for the neurophysiological dynamics underlying motor inhibitory control. *Human Brain Mapping*, *40*, 4253–4265.

Raftery, A. E. (1995). Bayesian model selection in social research. *Sociological Methodology*, *25*, 111–163.

Rushworth, M. F. S., Walton, M. E., Kennerley, S. W., & Bannerman, D. M. (2004). Action sets and decisions in the medial frontal cortex. *rends in Cognitive Sciences (Regul Ed)*, *8*, 410–417.

Stock, A.-K., Gohil, K., Huster, R. J., & Beste, C. (2017). On the effects of multimodal information integration in multitasking. *Scientific Reports*, *7*, 4927.

Stock, A.-K., Wascher, E., & Beste, C. (2013). Differential effects of motor Efference copies and proprioceptive information on response evaluation processes. Ed. François Tremblay. *PLoS ONE*, *8*, e62335.

Stürmer, B., Siggelkow, S., Dengler, R., & Leuthold, H. (2000). Response priming in the Simon paradigm. A transcranial magnetic stimulation study. *Experimental Brain Research*, *135*, 353–359.

Takacs, A., Mückschel, M., Roessner, V., & Beste, C. (2020). Decoding stimulus-response representations and their stability using EEG-based multivariate pattern analysis. *Cerebral Cortex Communications*, *1*, 1–12. https://doi.org/10.1093/texcom/tgaa016

Takacs, A., Zink, N., Wolff, N., Münchau, A., Mückschel, M., & Beste, C. (2020). Connecting EEG signal decomposition and response selection processes using the theory of event coding framework. *Human Brain Mapping*, *41*, 2862–2877.

Tandonnet, C., Garry, M. I., & Summers, J. J. (2011). Selective suppression of the incorrect response implementation in choice behavior assessed by transcranial magnetic stimulation. *Psychophysiology*, *48*, 462–469.

Tavor, I., Jones, O. P., Mars, R. B., Smith, S. M., Behrens, T. E., & Jbabdi, S. (2016). Task-free MRI predicts individual differences in brain activity during task performance. *Science*, *352*, 216–220.

Tosun, T., Berkay, D., Sack, A. T., Çakmak, Y. Ö., & Balcı, F. (2017). Inhibition of pre–supplementary motor area by continuous theta burst stimulation leads to more cautious decision-making and more efficient sensory evidence integration. *Journal of Cognitive Neuroscience*, *29*, 1433–1444.

Tsujimoto, T., Shimazu, H., & Isomura, Y. (2006). Direct recording of theta oscillations in primate prefrontal and anterior cingulate cortices. *Journal of Neurophysiology*, *95*, 2987–3000.

Tsujimoto, T., Shimazu, H., Isomura, Y., & Sasaki, K. (2010). Theta oscillations in primate prefrontal and anterior cingulate cortices in forewarned reaction time tasks. *Journal of Neurophysiology*, *103*, 827–843.

van Aerde, K. I., Mann, E. O., Canto, C. B., Heistek, T. S., Linkenkaer-Hansen, K., Mulder, A. B., … Mansvelder, H. D. (2009). Flexible spike timing of layer 5 neurons during dynamic beta oscillation shifts in rat prefrontal cortex. *Journal of Physiology (London)*, *587*, 5177–5196.

Verleger, R., Grauhan, N., & Śmigasiewicz, K. (2016). Is P3 a strategic or a tactical component? Relationships of P3 sub-components to response times in oddball tasks with go, no-go and choice responses. *NeuroImage*, *143*, 223–234.

Verleger, R., Kuniecki, M., Möller, F., Fritzmannova, M., & Siebner, H. R. (2009). On how the motor cortices resolve an inter-hemispheric response conflict: An event-related EEG potential-guided TMS study of the flankers task. *The European Journal of Neuroscience*, *30*, 318–326.

Verleger, R., Metzner, M. F., Ouyang, G., Śmigasiewicz, K., & Zhou, C. (2014). Testing the stimulus-to-response bridging function of the oddball-P3 by delayed response signals and residue iteration decomposition (RIDE). *NeuroImage*, *100*, 271–280.

Wang, C., Ulbert, I., Schomer, D. L., Marinkovic, K., & Halgren, E. (2005). Responses of human anterior cingulate cortex microdomains to error detection, conflict monitoring, stimulus-response mapping, familiarity, and orienting. *The Journal of Neuroscience*, *25*, 604–613.

Westerhausen, R., Moosmann, M., Alho, K., Belsby, S.-O., Hämäläinen, H., Medvedev, S., … Hugdahl, K. (2010). Identification of attention and cognitive control networks in a parametric auditory fMRI study. *Neuropsychologia*, *48*, 2075–2081.

Yordanova, J., Falkenstein, M., Hohnsbein, J., & Kolev, V. (2004). Parallel systems of error processing in the brain. *NeuroImage*, *22*, 590–602.

SUPPORTING INFORMATION

Additional supporting information may be found online in the Supporting Information section at the end of this article.

How to cite this article: Pscherer C, Bluschke A, Prochnow A, Eggert E, Mückschel M, Beste C. Resting theta activity is associated with specific coding levels in event-related theta activity during conflict monitoring. *Hum Brain Mapp*. 2020;41: 5114–5127. https://doi.org/10.1002/hbm.25178